ITERATIVE SPARSE DECONVOLUTION USING SEISLET-DOMAIN CONSTRAINT

MIN BAI and JUAN WU

Key Laboratory of Exploration Technology for Oil and Gas Resources of the Ministry of Education, Yangtze University, Wuhan 430100, P.R. China. baimin2016@126.com

ABSTRACT

Bai, M., and Wu, J., 2019. Iterative sparse deconvolution using seislet-domain constraint. *Journal of Seismic Exploration*, 28: 73-88.

Deconvolution can help improve the resolution of seismic data. We introduce a deconvolution formulation that can arbitrarily select the resolution level of the seismic data by defining a simple squeezing factor. Considering the ill-posedness of the deconvolution problem, some proper regularizations should be added when iteratively solving the deconvolution-related inverse problem. Traditionally used Fourier-domain constraint can be effective only when the seismic data contains linear events. We propose a seislet-domain constraint to regularize the deconvolution problem to deal with the curved events in seismic data. The seislet transform compressed the seismic data along structural direction, and thus can obtain the optimal sparsity. We apply the proposed method to both synthetic and field data examples and obtain encouraging performance.

KEY WORDS: deconvolution, noise attenuation, seislet transform, sparse inversion,
                regularization.

INTRODUCTION

The successful characterization of subsurface hydrocarbon reservoirs from seismic data highly depends on a clean and high-resolution seismic image. A lot of methods have been developed to improve the quality of seismic images. One widely used approach to improve seismic image is to apply some random noise attenuation approaches to remove the noise (either generated from the migration artifacts or from the ambient noise on the raw pre-stack seismic data) (Gan et al., 2016d; Zu et al., 2017a,b; Chen, 2018).

The simplest denoising method is by stacking the seismic data along the offset direction (Yang et al., 2015; Xie et al., 2017). By stacking the useful signals from multiple traces and multiple directions (e.g., offset and midpoint), the signal is enhanced while influence of noise is mitigated. Prediction based methods utilize the predictable property of useful signals to construct prediction filterers to enhance signals and reject noise, for example, f-x deconvolution (Canales, 1984), non-stationary predictive filtering (Liu et al., 2012; Liu and Chen, 2013). Sparse transform based approaches first transform seismic data to a sparse domain, then apply soft thresholding to the coefficients, finally transform the sparse coefficients back to the time-space domain. Widely used sparse transforms are Fourier transform (Zhong et al., 2016), curvelet transform (Zu et al., 2016), seislet transform (Gan et al., 2015b, 2016a; Wu et al., 2016; Gan et al., 2016b), Radon transform (Xue et al., 2016, 2017), and different types of wavelet transforms (Liu et al., 2016c,b). A recently popular transform is based on the machine learning engine to train adaptive transform basis in order to better deal with the complexity in various types of seismic data, which is called the dictionary learning based sparse transform (Chen, 2017; Siahsar et al., 2017a,b). Decomposition based approaches decompose the noisy seismic data into different components and then select the principal components to represent the useful signals. Empirical mode decomposition and its variations (Chen and Ma, 2014; Chen, 2016; Chen et al., 2016a, 2017b,d,a), variational mode decomposition (Liu et al., 2016a, 2017, 2018), singular value decomposition based approaches (Gan et al., 2015a), morphological component decomposition based approaches (Li et al., 2016a,b; Huang et al., 2017, 2018a), regularized non-stationary decomposition based approaches (Wu et al., 2018) are frequently used to extract the extract the useful components in multi-dimensional seismic data. Rank-reduction based approaches assume the seismic data to be low-rank after some data rearrangement steps (Bai et al., 2018). Such methods include the Cadzow filtering (Chen et al., 2016b,c; Zhang et al., 2017; Siahsar et al., 2017c), Mean and median filters utilize the statistical difference between signal and noise to reject the Gaussian white noise or impulsive noise (Gan et al., 2016c; Bai and Wu, 2017; Chen et al., 2017c; Huang et al., 2018b). Instead of proposing a standalone denoising strategy, Chen and Fomel (2015) proposed a two-step denoising approach that tries to solve a long-existing problem in almost all denoising approaches: the signal leakage problem. By proposing a new concept called local orthogonalization, Chen and Fomel (2015) retrieved the coherent signals from the removed noise section to guarantee no signal leakage in any denoising algorithms.

All the published methods have their own pros and cons regarding the denoising assumptions. Increasing the resolution of seismic data is also of great importance to seismic data processing. Seismic deconvolution is such as a process to uncover the subsurface reflectivity structure by removing the earth response from the data. In this paper, we first introduce a framework in which the noise attenuation problem and the resolution enhancing problem

are solved simultaneously (Chen and Jin, 2015). We first review the convolution model widely used in the traditional seismic deconvolution literature and then introduce a new inverse problem for simultaneously removing noise and increasing resolution. Considering the ill-posedness of the new inverse problem, a proper regularization should be applied. Traditionally used Fourier-domain sparsity constraint cannot be effective when the subsurface structure becomes complex (Chen and Jin, 2015; Bai and Wu, 2018). To deal with the curving reflector structure, we propose to apply the seislet-domain sparsity constraint to regularize the inverse problem. The seislet transform compresses the seismic data along the structural direction and thus can hopefully obtain the optimal sparsity for seismic data compared with the state-of-the-art algorithms. Bot synthetic and field data examples are used to demonstrate the superior performance of the proposed method.

THEORY

Deconvolution formulation

In the case that no random noise involved, the convolution model for post-stack seismic data can be expressed as:

$$\mathbf{d} = \mathbf{W}\mathbf{r} \quad , \tag{1}$$

where $\mathbf{d}$ denotes seismic data, note that the multi-dimensional seismic data has been reshaped into 1D vector in the formulation, $\mathbf{W}$ is the wavelet convolution operator and $\mathbf{r}$ is the subsurface reflectivity.

Suppose we can enhance the resolution of the seismic data by squeezing the wavelet, we can use the similar convolution model to denote the synthesized process:

$$\mathbf{d}_s = \mathbf{W}_s\mathbf{r} \quad , \tag{2}$$

where $\mathbf{d}_S$ denotes the squeezed seismic data, $\mathbf{W}_s$ is the convolution operator that is composed of the squeezed wavelet $w_s(t) = w(\lambda t)$. $w_s(t)$ and $w(t)$ denote the squeezed and the original wavelets, respectively. λ (> 1) is the squeezing factor. Usually we choose $\lambda = 4$ to balance the resolution enhancement and the interpretation difficulty.

In our formulation, the generalized deconvolution aims to obtain the data as if the real seismic wavelet is the squeezed wavelet, we can combine eqs. (1) and (2) and formulate the following equation:

$$\mathbf{d} = \mathbf{W}\mathbf{W}_s^{-1}\mathbf{d}_s \quad , \tag{3}$$

where $\mathbf{W}_s^{-1}$ denotes the deconvolution operator that is composed of the squeezed wavelet. The squeezed version of the original source wavelet. The squeezing process acts as the simplest form of the wavelet shaping step.

In reality, there is much random noise in the seismic data. Although, taking random noise into account, all eqs. (1), (2), and (3) will be modified, we can generally modify eq. (3) to summarize all the changes

$$\mathbf{d} = \mathbf{W}\mathbf{W}_s^{-1}\mathbf{d}_s + \mathbf{n} \quad , \tag{4}$$

where $\mathbf{n}$ denotes the random noise vector, which is unknown. Eq. (4) can be formulated into a classic form of inverse problem:

$$\mathbf{F}\mathbf{m} + \mathbf{n} = \mathbf{d} \quad , \tag{5}$$

where $\mathbf{F} = \mathbf{W}\mathbf{W}_s^{-1}$ denotes the forward operator, $\mathbf{m} = \mathbf{d}_S$ denotes the model, and $\mathbf{d}$ denotes the observed data. We now turn to solving inverse problem (5).

Inversion by shaping regularization

The shaping regularization Fomel (2007) can offer us much freedom in solving the inverse problem (5). The unknown $\mathbf{m}$ in eq. (5) can be recovered iteratively using the nonlinear shaping regularization:

$$\mathbf{m}_{n+1} = \mathcal{S}[\mathbf{m}_n + \mathbf{B}(\mathbf{d} - \mathbf{F}\mathbf{m}_n)] \quad , \tag{6}$$

where operator $\mathcal{S}$ shapes the estimated model into the space of more admissible models at each iteration Fomel (2007) and $\mathbf{B}$ is the backward operator that provides an inverse mapping from data space to model space. Daubechies et al. (2004) proved that, if $\mathcal{S}$ is a sparse domain nonlinear thresholding operator, $\mathbf{B} = \mathbf{F}^T$, where $\mathbf{F}^T$ is the adjoint operator of $\mathbf{F}$, iteration (6) converges to the solution of eq. (7) with a L_1 regularization term:

$$\min_{\mathbf{m}} \| \mathbf{F}\mathbf{m} - \mathbf{d} \|_2^2 + \mu \| \mathbf{A}^{-1}\mathbf{m} \|_1 \quad , \tag{7}$$

where μ is a controlling factor and $\mathbf{A}^{-1}$ denotes a sparsity-promoting transform.

The nonlinear operators S and $\mathbf{B}$ can be chosen as any combination of operators that can make the iteration converge. For example, S can be a coherency-promoting operator (Chen et al., 2014), or piecewise-constant layering constraint operator (Fomel, 2008). Thus, the shaping regularization framework is very flexible in solving inverse problem (5). The connections between linear shaping regularization (when S and $\mathbf{B}$ are both linear operators) and the Tikhonov regularization can be found in detail in Fomel (2007). More details about the nonlinear shaping regularization can be found in Fomel (2008).

In this paper, we adopt the shaping regularization framework 6 to solve the inverse problem. The shaping operator S is chosen as a transform domain thresholding operator. In order to set the optimal threshold, during each iteration, we set the threshold as the minimum of the p% largest coefficients. be introduced in detail in the next section. The backward operator $\mathbf{B}$ is chosen as the pseudo-inverse of $\mathbf{F}$, as suggested in Daubechies et al. (2008). However, the sparsity in the transform domain plays an important role in the final result. The Fourier-domain sparsity constraint is usually used for sparsity constraint, e.g., in (Abma and Kabir, 2006). However, we propose to use the seislet-domain sparsity constraint to regularize the inverse problem. In the next section, we will briefly introduce the seislet transform.

Brief review of the seislet transform

The seislet transform is based on the second-generate wavelet transform, which is defined with the help of the wavelet-lifting scheme (Sweldens, 1995) combined with local plane-wave destruction. The wavelet-lifting utilizes predictability of even traces from odd traces of 2D seismic data and finds a difference $\mathbf{r}$ between them, which can be expressed as:

$$\mathbf{r} = \mathbf{o} - \mathbf{P}\left[\mathbf{e}\right] \tag{8}$$

where $\mathbf{P}$ is the prediction operator. A coarse approximation $\mathbf{c}$ of the data can be achieved by updating the even component:

$$\mathbf{c} = \mathbf{e} + \mathbf{U}\left[\mathbf{r}\right] \tag{9}$$

where $\mathbf{U}$ is the updating operator.

The digital wavelet transform can be inverted by reversing the lifting-scheme operations as follows:

$$\mathbf{e} = \mathbf{c} - \mathbf{U}\,[\mathbf{r}] \quad , \tag{10}$$

$$\mathbf{o} = \mathbf{r} + \mathbf{P}\,[\mathbf{e}] \quad . \tag{11}$$

The forward transform starts with the finest scale (the original sampling) and goes to the coarsest scale. The inverse transfrom starts with the coarsest scale and goes back to the finest scale. At the start of forward transform, $\mathbf{e}$ and $\mathbf{o}$ corresponds to the even and odd traces of the data domain. At the start of the inverse transform, $\mathbf{c}$ and $\mathbf{r}$ will have just one trace of the coarsest scale of the seislet domain.

The above prediction and update operators can be defined, for example, as follows:

$$\mathbf{P}\,[\mathbf{e}]_k = \left(\mathbf{P}_k^{(+)}\,[\mathbf{e}_{k-1}] + \mathbf{P}_k^{(-)}\,[\mathbf{e}_k]\right)/2 \quad , \tag{12}$$

and

$$\mathbf{U}\,[\mathbf{r}]_k = \left(\mathbf{P}_k^{(+)}\,[\mathbf{r}_{k-1}] + \mathbf{P}_k^{(-)}\,[\mathbf{r}_k]\right)/4 \quad , \tag{13}$$

where $\mathbf{P}_k^{(+)}$ and $\mathbf{P}_k^{(-)}$ are operators that predict a trace from its left and right neighbors, correspondingly, by shifting seismic events according to their local slopes. This scheme is analogous to CDF biorthogonal wavelets (Cohen et al., 1992). The predictions need to operate at different scales, which means different separation distances between traces. Taken through different scales, eqs. (8)-(13) provide a simple definition for the 2D seislet transform. More accurate versions are based on other schemes for the digital wavelet transform (Liu et al., 2009).

EXAMPLES

We use two synthetic examples to demonstrate the performance of different methods, one being relatively simple and one being relatively complex. The first example is the well-known wedge model, as shown in Fig. 1a. The data after deconvolution using the Fourier-domain sparsity constraint is shown in Fig. 1b. The data after deconvolution using the seislet domain sparsity constraint is shown in Fig. 1c. It is obvious that the strong noise has been removed effectively and the resolution has been

enhanced greatly, and more importantly, the two deconvolved data are almost the same. We can get an initial conclusion that for relatively simple structure (i.e., linear events), the Fourier method and the seislet method can obtain similar results. We estimated the wavelet by stacking part of the data along the spatial dimension. The estimated wavelet is shown in Fig. 2a. The squeezed wavelet using a squeezing factor $\lambda = 4$ is shown in Fig. 2b. Fig. 3 shows a single-trace comparison between the original data and the data using different approaches. The comparison further confirms that the two methods are very close in this example.

(a)

(b)

(c)
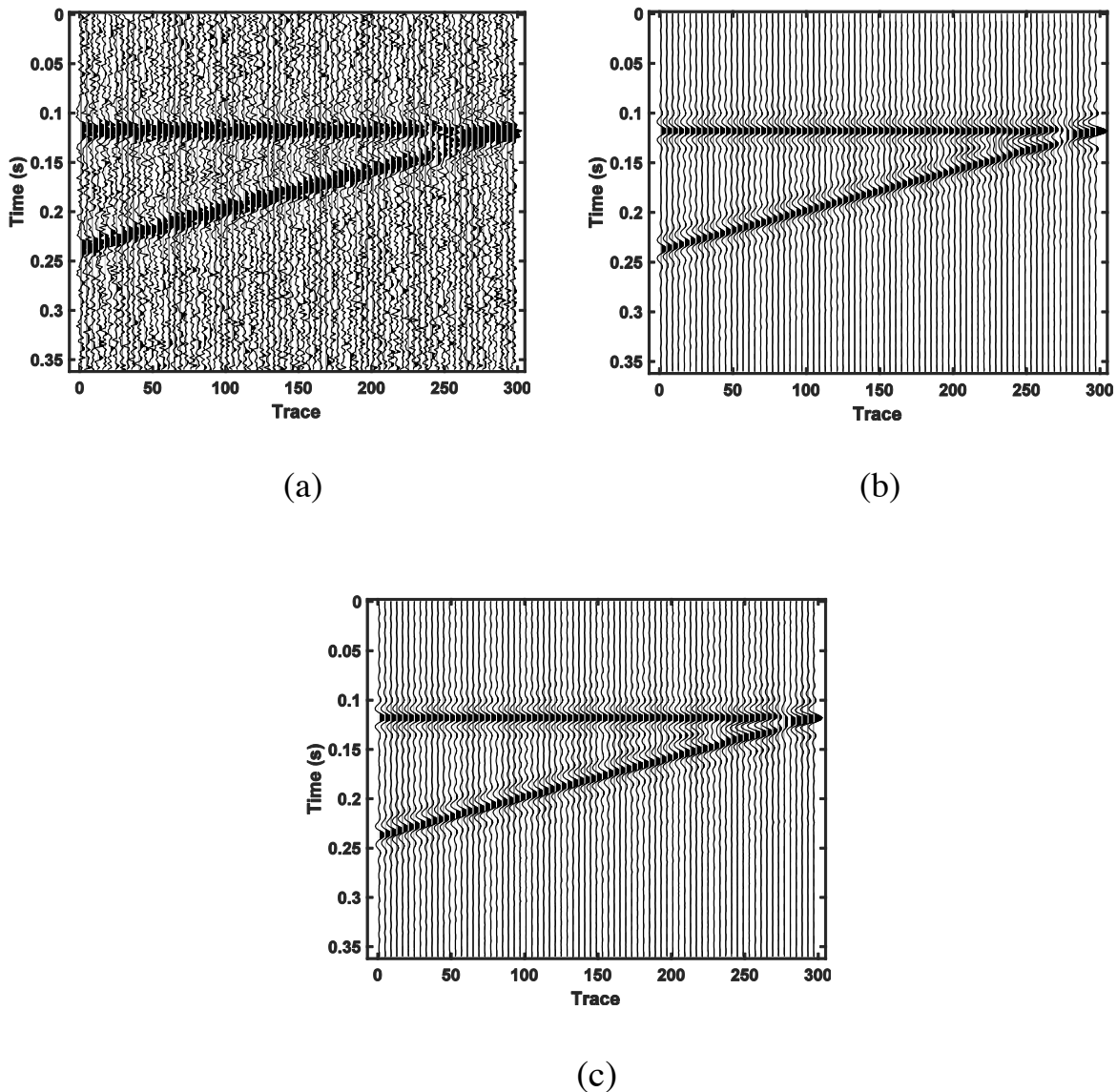
Fig. 1. The first synthetic data example (the wedge model). (a) Noisy data.
(b) Deconvolved data using the Fourier-domain sparsity constraint.
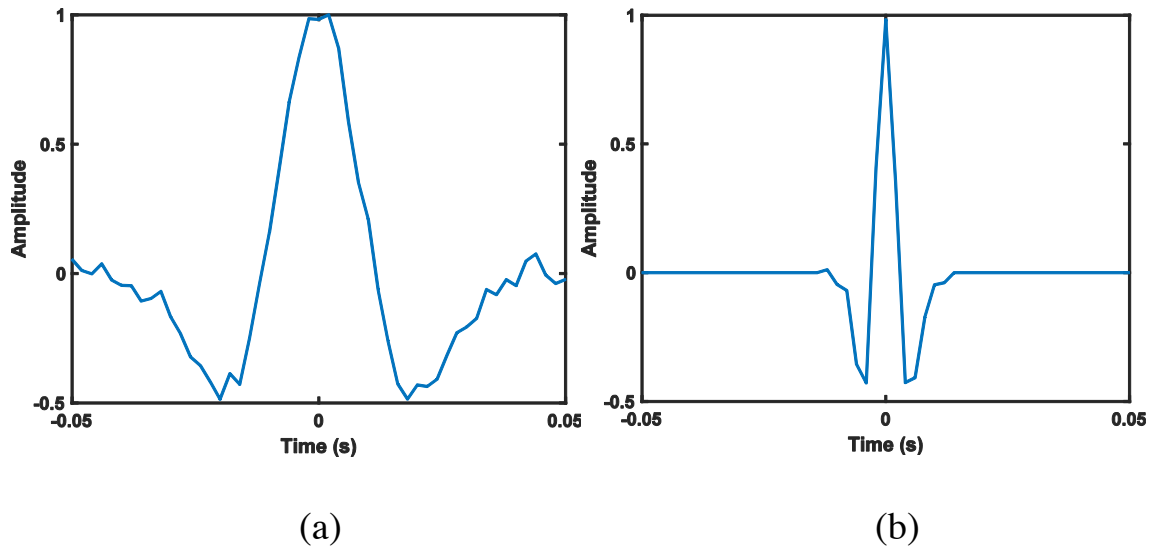(c) Deconvolved data using the seislet-domain sparsity constraint.

Fig. 2. The first synthetic data example (the wedge model). (a) Estimated wavelet and (b) the squeezed wavelet.
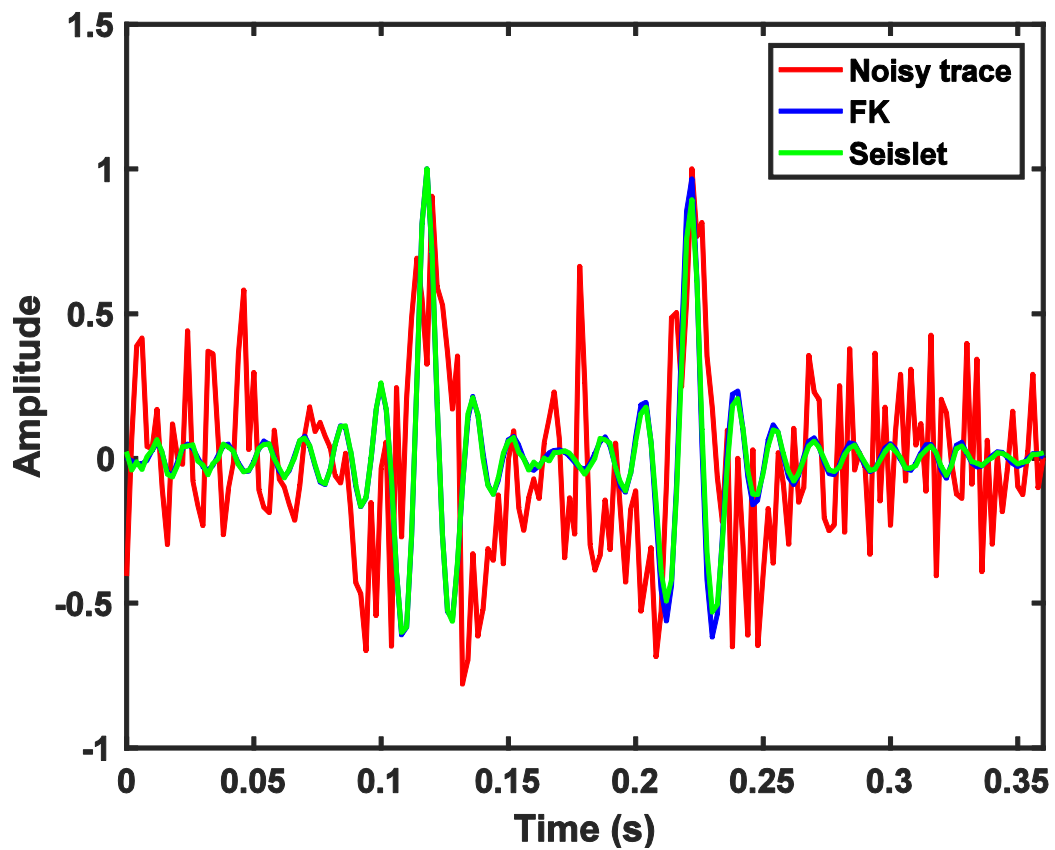

Fig. 3. Single-trace comparison of the first synthetic data example.

The second example is a slightly different model but is more complex. The model is shown in Fig. 4a. As can be seen in Fig. 4a, there is a curving event in the current model. The Fourier-domain method removes a lot of curving energy, as can be seen in Fig. 4b. The proposed method, however, preserves the curving event well, as seen in Fig. 4c. We also show a spectrum comparison in Fig. 5. It is obvious that the deconvolved data both have wider spectrum than the raw data. Besides, the proposed seislet constraint preserves the curving signal energy much better than the Fourier-domain constraint.
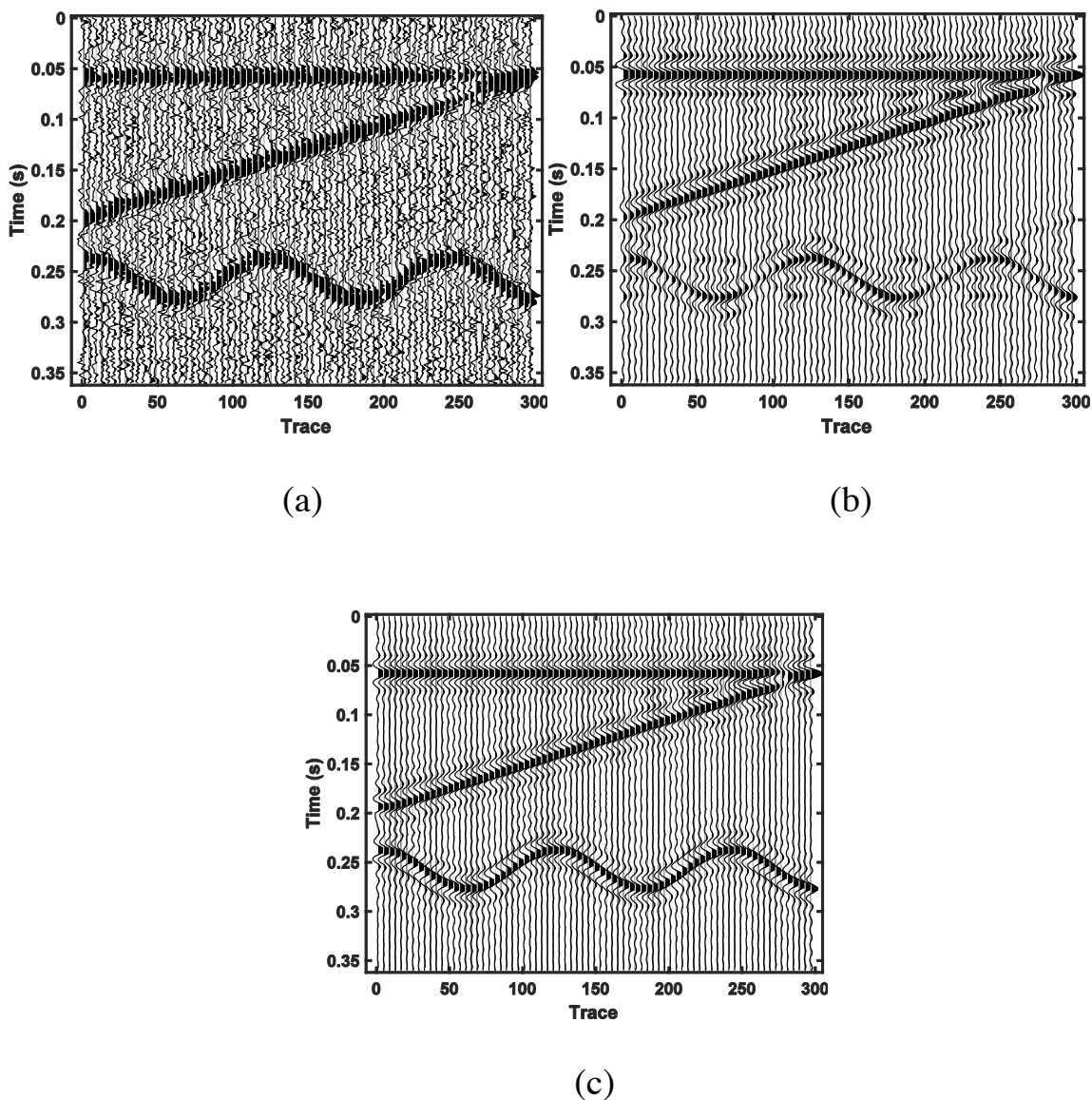

(a)

(b)

(c)

Fig. 4. The second synthetic data example. (a) Noisy data. (b) Deconvolved data using the Fourier-domain sparsity constraint. (c) Deconvolved data using the seislet-domain sparsity constraint.
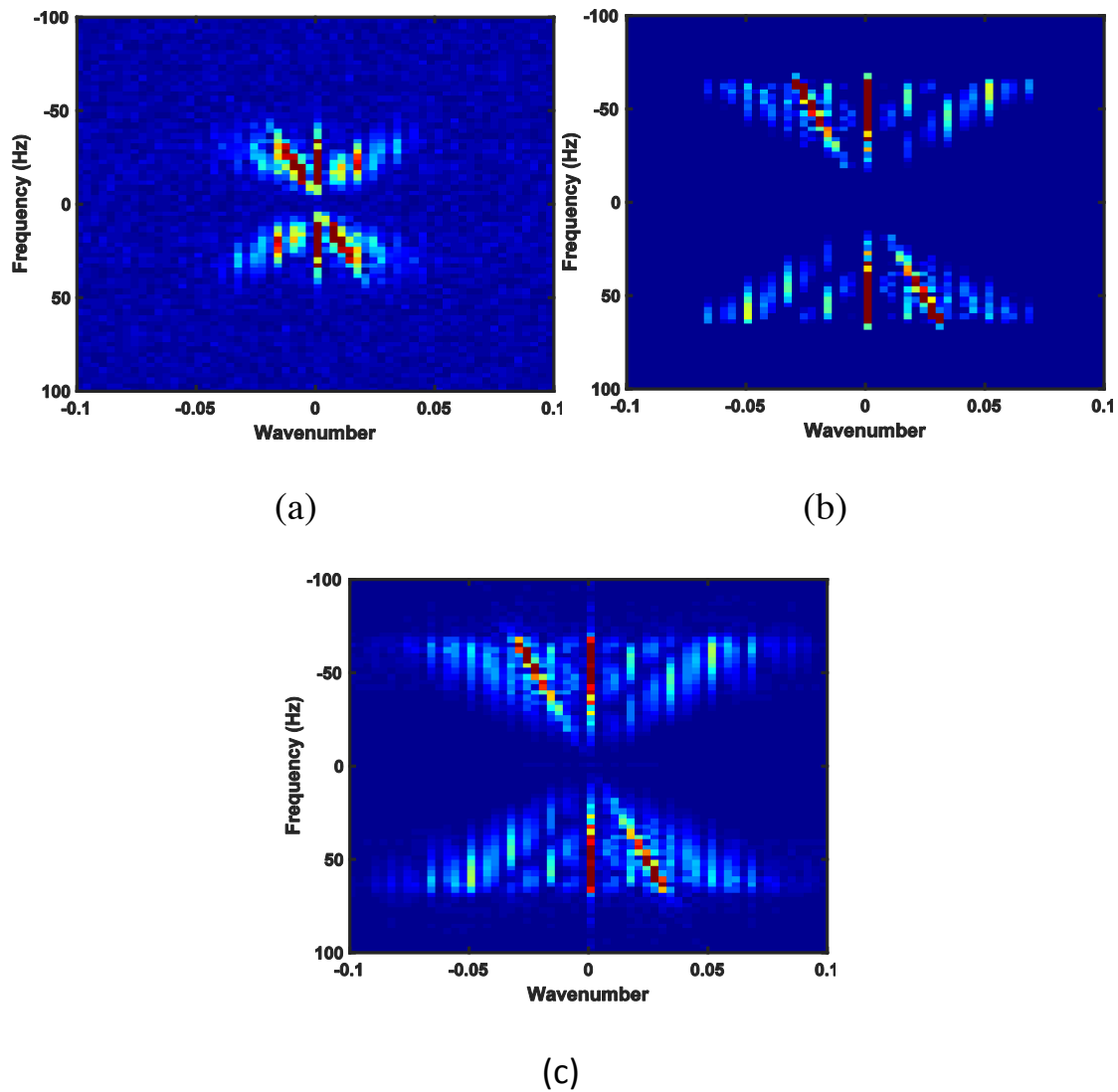
(a)

(b)

(c)

Fig. 5. Spectrum comparison of the second synthetic data example. (a) Noisy data.
(b) Deconvolved data using the Fourier-domain sparsity constraint. (c) Deconvolved data
using the seislet-domain sparsity constraint. Note the spectrum whitening and the well
preserved signal energy in the spectrum using the proposed method.

Fig. 6 shows a single-trace comparison between the original data
and the data using different approaches, which clearly demonstrates that
the blue line (corresponding to the Fourier method) and the green line
(corresponding to the seislet method) deviate a lot.

The next example is a land post-stack seismic section, as shown in
Fig. 7a. The deconvolved results using the two methods are shown in Figs.
7b and 7c, respectively. It is clear that the Fourier-domain constraint
method removes a lot of details of the data while the proposed seislet-
domain constraint preserves the curving details very well. Although there

seems to be an amplitude banding issue in the result, the proposed method is more convincing, as inferred from the synthetic test. For a better comparison, we zoomed three sections from different data in Fig. 7 and show them in Fig. 8. It is salient that the results from the Fourier-domain constraint contain almost flat events while the curving events are maintained well using the seislet-domain constraint.
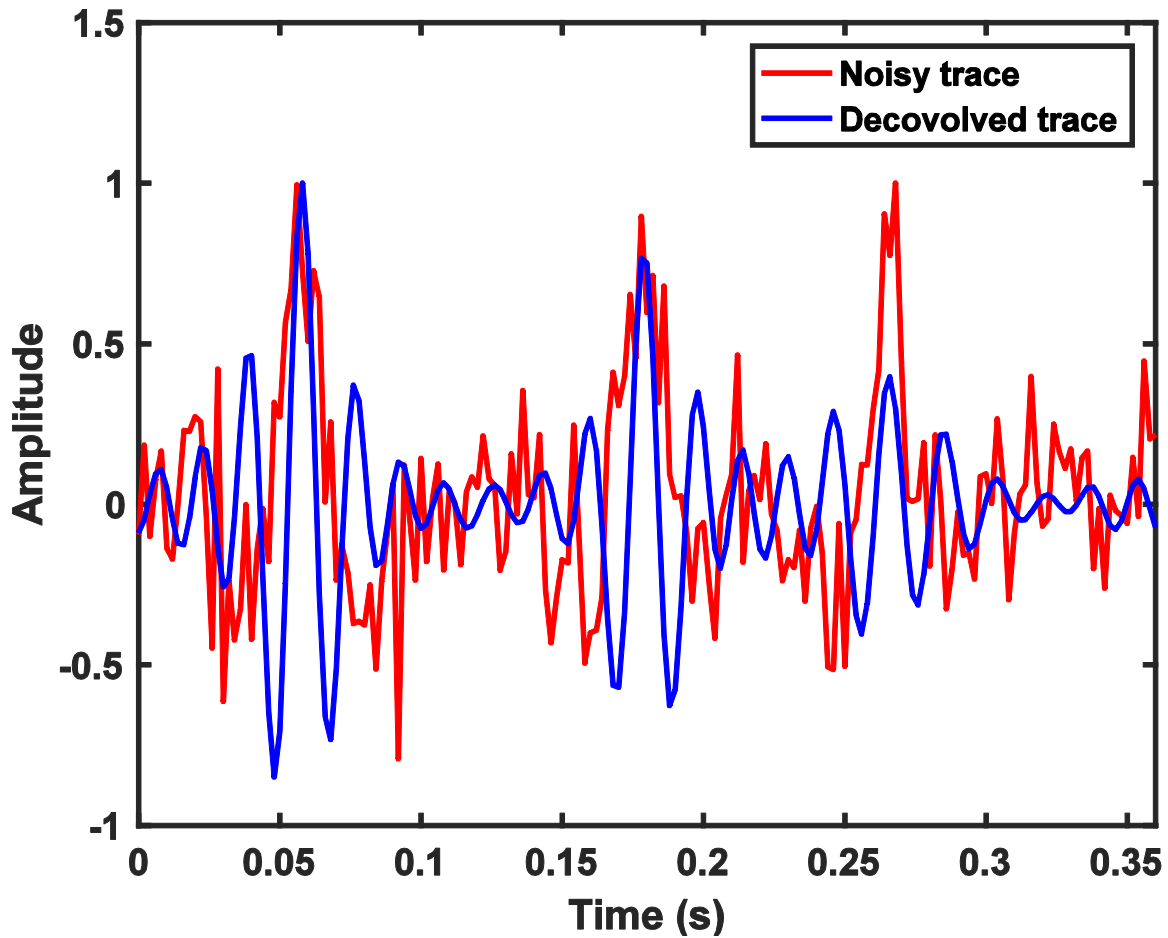
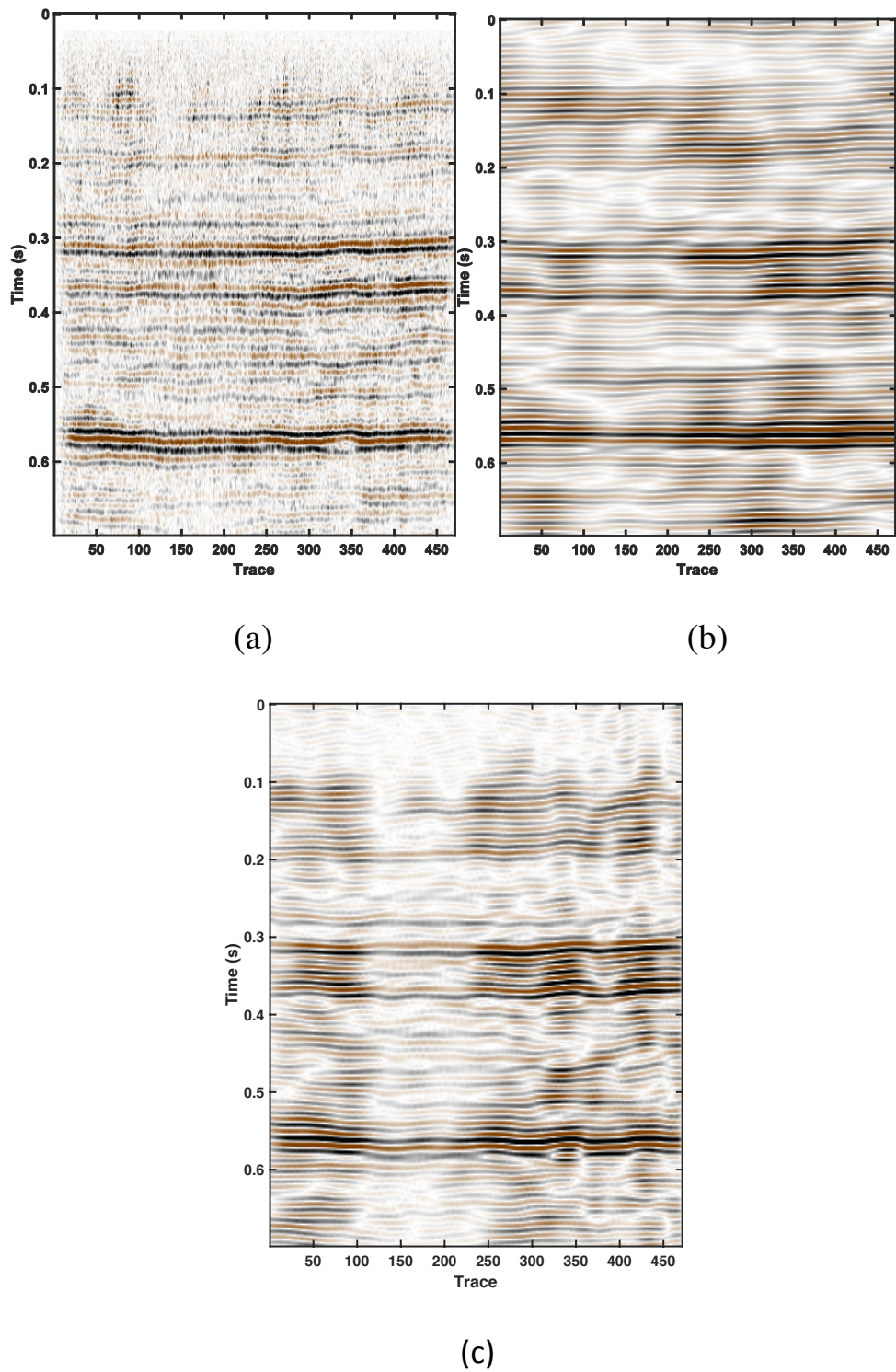Fig. 6. Single-trace comparison of the second synthetic data example.

(a)

(b)

(c)

Fig. 7. The field data example. (a) Field data. (b) Deconvolved data using the Fourier domain sparsity constraint. (c) Deconvolved data using the seislet-domain sparsity constraint.
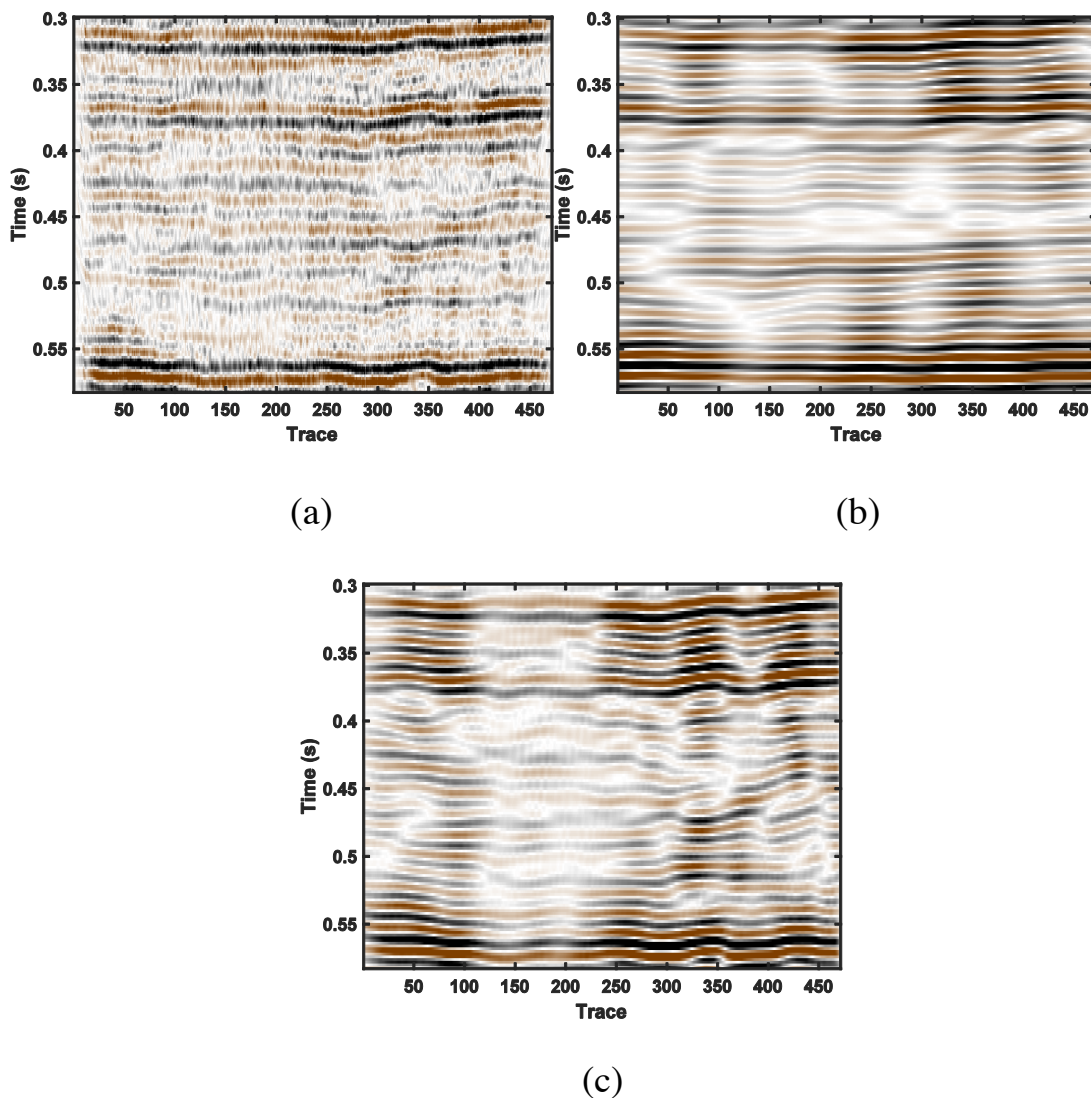
(a)

(b)

(c)

Fig. 8. The field data example (zoomed comparison). (a) Field data. (b) Deconvolved data using the Fourier-domain sparsity constraint. (c) Deconvolved data using the seislet domain sparsity constraint.

CONCLUSIONS

We have proposed a novel regularization method for constraining iterative deconvolution. The regularization is applied using the shaping regularization framework and a seislet domain sparsity constraint. Compared with the Fourier-domain sparsity constraint, the seislet-domain constraint can help the inversion preserve curving reflection events. The wedge model shows that in structurally simple data, the proposed method can obtain the similar performance as the Fourier-domain constraint method. However, for more complicated data, the proposed method outperforms the traditional method. The field data example further demonstrates the superior performance of the seislet-domain constraint to the traditional Fourier-domain constraint.

ACKNOWLEDGEMENTS

REFERENCES

Abma, R. and Kabir, N., 2006. 3D interpolation of irregular data with a POCS algorithm. Geophysics, 71: E91-E97.

Bai, M. and Wu, J., 2017. Effcient deblending using median filtering without correct normal moveout - with comparison on migrated images. J. Seismic Explor., 26: 455-479.

Bai, M. and Wu, J., 2018. Seismic deconvolution using iteartive transform-domain sparse inversion. J. Seismic Explor., 27: 103-116.

Bai, M., Wu, J., Xie, J. and Zhang, D., 2018. Least-squares reverse time migration of blended data with low-rank constraint along structural direction. J. Seismic Explor, 27: 29-48.

Canales, L., 1984. Random noise reduction. Expanded Abstr., 54th Ann. Internat. SEG Mtg., Atlanta: 525-527.

Chen, W., Chen, Y. and Cheng, Z., 2017a. Seismic time-frequency analysis using an improved empirical mode decomposition algorithm. J. Seismic Explor., 26: 367-380.

Chen, W., Chen, Y. and Liu, W., 2016a. Ground roll attenuation using improved complete ensemble empirical mode decomposition. J. Seismic Explor., 25: 485-495.

Chen, W., Xie, J., Zu, S., Gan, S. and Chen, Y., 2017b. Multiple reflections noise attenuation using adaptive randomized-order empirical mode decomposition. IEEE Geosci. Remote Sens. Lett., 14: 18-22.

Chen, W., Yuan, J., Chen, Y. and Gan, S., 2017c. Preparing the initial model for iterative deblending by median filtering. J. Seismic Explor., 26: 25-47.

Chen, W., Zhang, D. and Chen, Y., 2017d. Random noise reduction using a hybrid method based on ensemble empirical mode decomposition. J. Seismic Explor., 26: 227-249.

Chen, Y., 2016. Dip-separated structural filtering using seislet thresholding and adaptive empirical mode decomposition based dip filter. Geophys. J. Internat., 206: 457-469.

Chen, Y., 2017. Fast dictionary learning for noise attenuation of multidimensional seismic data. Geophys. J. Internat., 209: 21-31.

Chen, Y., 2018. Non-stationary least-squares complex decomposition for microseismic noise attenuation. Geophys. J. Internat., 213: 1572-1585.

Chen, Y. and Fomel, S., 2015. Random noise attenuation using local signal-and-noise orthogonalization. Geophysics, 80(6): WD1-WD9.

Chen, Y., Fomel, S. and Hu, J., 2014. Iterative deblending of simultaneous-source seismic data using seislet-domain shaping regularization. Geophysics, 79(5): V179-V189.

Chen, Y. and Jin, Z., 2015. Simultaneously removing noise and increasing resolution of seismic data using waveform shaping. IEEE Geosci. Remote Sens. Lett., 13: 102-104.

Chen, Y. and Ma, J., 2014. Random noise attenuation by f-x empirical mode decomposition predictive filtering. Geophysics, 79: V81-V91.

Chen, Y., Zhang, D., Huang, W. and Chen, W., 2016b. An open-source matlab code package for improved rank-reduction 3D seismic data denoising and reconstruction. Comput. Geosci., 95: 59-66.

Chen, Y., Zhang, D., Jin, Z., Chen, X., Zu, S., Huang, W. and Gan, S., 2016c. Simultaneous denoising and reconstruction of 5D seismic data via damped rank-reduction method. Geophys. J. Internat., 206: 1695-1717.

Cohen, A., Daubechies, I. and Feauveau, J.C., 1992. Biorthogonal bases of compactly supported wavelets. Communic. Pure Appl. Mathemat., 45: 485-560.

Daubechies, I., Defrise, M. and Mol, C.D., 2004. An iterative thresholding algorithm for linear inverse problems with a sparsity constraint. Comm. Pure Appl. Mathemat., 57: 1413-1457.

Daubechies, I., Fornasier, M. and Loris, I., 2008. Accelerated projected gradient method for linear inverse problems with sparsity constraints. J. Fourier. Analys. Applic., 14: 764-792.

Fomel, S., 2007. Shaping regularization in geophysical-estimation problems. Geophysics, 72: R29-R36.

Fomel, S., 2008. Nonlinear shapping regularization in geophysical inverse problems. Expanded Abstr., 78th Ann. Internat. SEG Mtg., Las Vegas: 2046-2051.

Gan, S., Chen, Y., Zu, S., Qu, S. and Zhong, W., 2015a. Structure-oriented singular value decomposition for random noise attenuation of seismic data. J. Geophys. Engineer.,12: 262-272.

Gan, S., Wang, S., Chen, Y. and Chen, X., 2016a. Simultaneous-source separation using iterative seislet-frame thresholding. IEEE Geosci. Remote Sens. Lett., 13: 197-201.

Gan, S., Wang, S., Chen, Y., Chen, X., Huang, W. and Chen, H., 2016b. Compressive sensing for seismic data reconstruction via fast projection onto convex sets based on seislet transform. J. Appl. Geophys., 130: 194-208.

Gan, S., Wang, S., Chen, Y., Chen, X. and Xiang, K., 2016c. Separation of simultaneous sources using a structural-oriented median filter in the flattened dimension. Comput. Geosci., 86: 46-54.

Gan, S., Wang, S., Chen, Y., Qu, S. and Zu, S., 2016d. Velocity analysis of simultaneous source data using high-resolution semblance-coping with the strong noise. Geophys. J. Internat., 204: 768-779.

Gan, S., Wang, S., Chen, Y., Zhang, Y. and Jin, Z., 2015b. Dealiased seismic data interpolation using seislet transform with low-frequency constraint. IEEE Geosci. Remote Sens. Lett., 12: 2150-2154.

Huang, W., R. Wang, and Y. Chen, Y., 2018a. Regularized non-stationary morphological reconstruction algorithm for weak signal detection in micro-seismic monitoring: Methodology. Geophys. J. Internat.,, 213: 1189-1211.

Huang, W., Wang, R., Gong, X. and Chen, Y., 2018b. Iterative deblending of simultaneous source seismic data with structuring median constraint. IEEE Geosci. Remote Sens. Lett., 15: 58-62.

Huang, W., Wang, R., Zu, S. and Chen, Y., 2017. Low-frequency noise attenuation in seismic and microseismic data using mathematical morphological filtering. Geophys. J. Internat., 211: 1318-1340.

Li, H., Wang, R., Cao, S., Chen, Y. and Huang, W., 2016a. A method for low-frequency noise suppression based on mathematical morphology in microseismic monitoring. Geophysics, 81(3): V159-V167.

Li, H., Wang, R., Cao, S., Chen, Y., Tian, N. and Chen, X., 2016b. Weak signal detection using multiscale morphology in microseismic monitoring. J. Appl. Geophys.,133: 39-49.

Liu, G. and Chen, X., 2013. Noncausal f-x-y regularized nonstationary prediction filtering for random noise attenuation on 3D seismic data. J. Appl. Geophys., 93:60-66.

Liu, G., Chen, X., Du, J. and Wu, K., 2012. Random noise attenuation using f-x regularized nonstationary autoregression. Geophysics, 77: V61-V69.

Liu, W., Cao, S. and Chen, Y., 2016a. Applications of variational mode decomposition in seismic time-frequency analysis. Geophysics, 81(5): V365-V378.

Liu, W., Cao, S. and Chen, Y., 2016b. Seismic time-frequency analysis via empirical wavelet transform. IEEE Geosci. Remote Sens. Lett., 13: 28-32.

Liu, W., Cao, S., Jin, Z., Wang, Z. and Chen, Y., 2018. A novel hydrocarbon detection approach via high-resolution frequency-dependent AVO inversion based on variational mode decomposition. IEEE Transact. Geosci. Remote Sens., 56: 2007-2024.

Liu, W., Cao, S., Liu, Y. and Chen, Y., 2016c. Synchrosqueezing transform and its applications in seismic data analysis. J. Seismic Explor., 25: 27-44.

Liu, W., Cao, S., Wang, Z., Kong, X. and Chen, Y., 2017. Spectral decomposition for hydrocarbon detection based on VMD and Teager-Kaiser energy. IEEE Geosci. Remote Sens. Lett., 14: 539-543.

Liu, Y., Fomel, S., Liu, C., Wang, D., Liu, G. and Feng, X., 2009. High-order seislet transform and its application of random noise attenuation. Chin. J. Geophys., 52: 2142-2151.

Siahsar, M.A.N., Abolghasemi, V. and Chen, Y., 2017a. Simultaneous denoising and interpolation of 2D seismic data using data-driven non-negative dictionary learning. Sign. Process., 141: 309-321.

Siahsar, M.A.N., Gholtashi, S., Kahoo, A.R., Chen, W. and Chen, Y., 2017b. Data-driven multi-task sparse dictionary learning for noise attenuation of 3D seismic data. Geophysics, 82(6): V385-V396.

Siahsar, M.A.N., Gholtashi, S., Olyaei, E., Chen, W. and Chen, Y., 2017c. Simultaneous denoising and interpolation of 3D seismic data via damped data-driven optimal singular value shrinkage. IEEE Geosci. Remote Sens. Lett., 14: 1086-1090.

Sweldens, W., 1995. Lifting scheme: A new philosophy in biorthogonal wavelet constructions. Wavelet applications in signal and image processing iii. Proc. SPIE 2569: 68-79.

Wu, G., Fomel, S. and Chen, Y., 2018. Data-driven time-frequency analysis of seismic data using non-stationary prony method. Geophys. Prosp., 66: 85-97.

Wu, J., Wang, R., Chen, Y., Zhang, Y., Gan, S. and Zhou, C., 2016. Multiples attenuation using shaping regularization with seislet domain sparsity constraint. J. Seismic Explor., 25: 1-9.

Xie, J., Chen, W., Zhang, D., Zu, S. and Chen, Y., 2017. Application of principal component analysis in weighted stacking of seismic data. IEEE Geosci. Remote Sens. Lett., 14: 1213-1217.

Xue, Y., Man, M., Zu, S., Chang, F. and Chen,Y., 2017. Amplitude-preserving iterative deblending of simultaneous source seismic data using high-order Radon transform. J. Appl. Geophys., 139: 79-90.

Xue, Y., Yang, J., Ma, J. and Chen, Y., 2016. Amplitude-preserving nonlinear adaptive multiple attenuation using the high-order sparse Radon transform. J. Geophys. Engineer., 13: 207-219.

Yang, W., Wang, R., Wu, J., Chen, Y., Gan, S. and Zhong, W., 2015. An efficient and effective common reflection surface stacking approach using local similarity and plane wave flattening. J. Appl. Geophys., 117: 67-72.

Zhang, D., Zhou, Y., Chen, H., Chen, W., Zu, S. and Chen, Y., 2017. Hybrid rank-sparsity constraint model for simultaneous reconstruction and denoising of 3D seismic data. Geophysics, 82(5): V351-V367.

Zhong, W., Chen, Y., Gan, S. and Yuan, J., 2016. L1/2 norm regularization for 3D seismic data interpolation. J. Seismic Explor., 25: 257-268.

Zu, S., Zhou, H., Chen, Y., Qu, S., Zou, X., Chen, H. and Liu, R., 2016. A periodically varying code for improving deblending of simultaneous sources in marine acquisition. Geophysics, 81(3): V213-V225.

Zu, S., Zhou, H., Li, Q., Chen, H., Zhang, Q., Mao, W. and Chen, Y., 2017a. Shot-domain deblending using least-squares inversion. Geophysics, 82(4): V241-V256.

Zu, S., Zhou, H., Mao, W., Zhang, D., Li, C., Pan, X. and Chen, Y., 2017b. Iterative deblending of simultaneous-source data using a coherency-pass shaping operator. Geophys. J. Internat., 211: 541-557.